Computers and Mathematics with Applications 67 (2014) 340–349

Contents lists available at ScienceDirect

Computers and Mathematics with Applications

journal homepage: www.elsevier.com/locate/camwa

Three-dimensional LBE simulations of a decay of liquid dielectrics with a solute gas into the system of gas–vapor channels under the action of strong electric fields☆

A.L. Kupershtokh*

Lavrentyev Institute of Hydrodynamics SB RAS, Novosibirsk, Russia

ARTICLE INFO

Keywords:
Lattice Boltzmann equation method
Phase transition
Dynamics of multiphase media
Computer simulations
Parallel computations
Graphics processing units

ABSTRACT

The three-dimensional simulations of an anisotropic decay of binary mixtures of a dielectric liquid with solute gas in a strong electric field are carried out. The Lattice Boltzmann Equation method (LBE) is exploited for computer simulations of the evolution of such systems with the newly arising interfaces between vapor and liquid phases. The parallel implementation of the LBE algorithm is realized on a large number of cores in the GPU. For the GPU programming, the CUDA technology is used.

It is important that new regions of the low-density phase appear as thin quasi-cylindrical gas–vapor channels oriented along the electric field. The gas–vapor channels expand because of the diffusion of the solute gas from the mixture, evaporation of liquid into the channels and also due to the coalescence of channels with each other. The critical values of electric field necessary for such decay of a binary mixture are considerably lower than the critical electric field for pure dielectric liquids. Hence, if we take into account a solute gas, the electric fields for which the anisotropic mechanism of streamer channels generation and growth is operated, become considerably lower.

Thus, at a breakdown of dielectric liquids in a strong electric field, the anisotropic instability is possibly the key mechanism of the generation of a gas phase, inception of conducting streamer structures, their fast growth in the form of thin filamentary channels, as well as branching of streamer structures during propagation.

1. Introduction

The main features of the well-known phenomenon of breakdown of liquid dielectrics are tree- or bush-like shapes of conductive structures (streamers), a cylindrical form of channel segments, and ultra-fast propagation of streamer tips in a strong electric field with a velocity of up to 300 km/s [1,2]. However, the mechanisms of a streamer inception and a fast propagation of streamer filaments were not revealed till now. Since the electric strength of a liquid phase is very high, the electric breakdown can occur initially in a low-density phase (vapor). For dielectric liquids with nonlinear density dependence of permittivity, the new mechanism of anisotropic decay of an initially uniform fluid being in a stable liquid state into the liquid and gaseous phases under the action of strong electric fields was proposed in works [3,4]. It is important

☆ This work was supported in part by the Russian Foundation for Basic Research (No. 13-08-00763), by the grant of the President of the Russian Federation (No. NSh–247.2012.1), and by the Siberian Branch of Russian Academy of Sciences (Project No. 79–2012).

* Tel.: +7 383 3361163; fax: +7 383 3333332.
E-mail addresses: skn@hydro.nsc.ru, sknew@mail.ru.

0898-1221/$ – see front matter © 2013 Elsevier Ltd. All rights reserved.
http://dx.doi.org/10.1016/j.camwa.2013.08.030

that new segments of the low-density phase appear in the form of thin filamentary channels oriented on average along the electric field. The mechanism of the anisotropic decay allows one to explain easily the major part of the experimentally observed phenomena at liquid dielectric breakdowns [5] (an ultra-fast propagation of streamer tips, an occurrence of a fan of dark thin radial channels of low density near the tip of the electrode and a further breakdown of the gas phase in one or several of these channels, the cylindrical shape of segments of channels and also their branching during propagation). The authors of experimental work [5] explained their results on the breakdown of liquid dielectrics based on our model of streamer inception and growth according to the mechanism of anisotropic decay of liquid dielectrics in a high electric field proposed in [3,6]. However, the first study was carried out only for pure dielectric liquids. In this case, the anisotropic decay can occur for electric fields of the magnitudes of the order of tens of MV/cm. On the other hand, the actual electric fields in most experiments on electrical breakdowns were much lower (in the range from several tenths to several MV/cm). Moreover, the first computer simulations were carried out only in the two-dimensional case.

In the present study, the three-dimensional simulations of anisotropic decay of binary mixtures of a dielectric liquid with solute gas in a strong electric field were carried out. For binary mixtures of a dielectric liquid and a solute gas, the value of the critical electric field turned out to be considerably lower than for the pure dielectric liquids. At the breakdown of dielectric liquids in a strong electric field, this anisotropic instability is possibly the key mechanism of generation of a gas phase, inception of conducting streamer structures, their fast growth in the form of thin filamentary channels and the branching of streamer structures during propagation.

The Lattice Boltzmann Equation (LBE) method was used for three-dimensional computer simulations of the evolution of such binary systems in strong electric fields with the newly arising interfaces between vapor and liquid phases. This method has been widely exploited in simulations of multiphase and multicomponent flows.

The several LBE models are known to simulate multiphase flows (including the color-fluid model [7], the free energy model [8], the model with interparticle interaction forces [9], and the pseudopotential model [10]). The major disadvantage of the color-fluid model is that it does not include any equation of state. Hence, this model cannot describe the phase transitions, the origination of new interfaces, condensation and evaporation. The free energy model ensures the constant interface thickness. However, this model is more complicated, needs corrections of equilibrium distribution functions to improve the Galilean invariance, does not describe the correct temperature dependence of the surface tension and cannot simulate the liquid–vapor interfaces with a high density ratio.

The model exploited in the present paper was firstly proposed in 2005–2007 [11–13]. It was based on two models. The main one was the pseudopotential model proposed by Qian [10]. We exploited this approach, because it allows one to incorporate easily an arbitrary form of EOS. However, the part of the finite difference isotropic approximation of the gradient of the pseudopotential was very close to the model of interparticle interaction [9].

The idea to introduce the total force acting on a node instead of interparticle forces was proposed in the work [10]. The total force should be a gradient of a pseudopotential $\mathbf{F} = -\nabla U$, where $U(\rho) = P(\rho) - \rho\theta$. Later, this approach was extended to the equation of state given in the form $P(\rho, T)$ [14]. In [11–13], the special function $\Phi = \sqrt{-U}$ was introduced that allowed us to propose a new isotropic finite difference approximation of the gradient of the pseudopotential.

Later, in 2011, the same model was published in [15]. If one redefines the free coefficients of this model, their main equations exactly coincide with the equations proposed earlier in [11–13].

A modern Graphics Processing Unit (GPU) consists of a large number of cores that allows one to realize parallel computations. For the first time, a GPU was used for LBE simulations in the work [16]. For simple variants of LBE without phase transitions, the parallel computations using one or several GPU were exploited in [16–20]. Multiphase lattice Boltzmann simulations of fluid flows were carried out in [21,22].

This paper is organized as follows. In Section 2, the macroscopic equations are given that describe the hydrodynamics of the problem and the electric field distribution. In Section 3, the algorithm of the LBE method for simulation of a fluid with a possible liquid–vapor phase transition in accordance with the given equation of state is described. Section 4 is devoted to parallel computations on Graphics Processing Units (GPU). Section 5 is devoted to the simulations of spinodal decomposition using the lattice Boltzmann equation method. In Section 6, the simulations of a decay of binary mixtures in strong electric fields are described. Some concluding remarks are given in Section 7.

2. Macroscopic equations

The well-known macroscopic equations of hydrodynamics for a viscous compressible fluid are the continuity equation

$$\frac{\partial \rho}{\partial t} + \nabla(\rho \mathbf{u}) = 0 \tag{1}$$

and the Navier–Stokes equation

$$\frac{\partial(\rho u_i)}{\partial t} + \frac{\partial \Pi_{ij}^{(0)}}{\partial x_j} = \rho a_i + \frac{\partial}{\partial x_j}\left(\mu\left(\frac{\partial u_i}{\partial x_j} + \frac{\partial u_j}{\partial x_i}\right)\right) + \frac{\partial}{\partial x_j}\left(\left(\lambda - \frac{2}{3}\mu\right)\delta_{ij}\frac{\partial u_k}{\partial x_k}\right). \tag{2}$$

Here, ρ is the density, $\mathbf{u}$ is the velocity, μ and λ are the dynamic and second viscosities, and $\Pi_{ij}^{(0)} = P(\rho, T)\delta_{ij} + \rho u_i u_j$ is the non-viscous part of the momentum flux tensor. The acceleration $\mathbf{a}$ is defined by the total body force $\mathbf{F} = \rho\mathbf{a}$. The equation

of state is in the form $P(\rho, T)$ that allows one to simulate the vapor–liquid phase transition. The stress tensor has the form

$$\sigma_{ij} = -P\delta_{ij} + \mu\left(\frac{\partial u_i}{\partial x_j} + \frac{\partial u_j}{\partial x_i}\right) + \left(\lambda - \frac{2}{3}\mu\right)\delta_{ij}\frac{\partial u_k}{\partial x_k}.$$

Two boundary conditions should be satisfied at each element S of interfaces between phases of densities ρ' and ρ''. If the mass flux through the interface is absent, the kinematical condition

$$\mathbf{u}' = \mathbf{u}''$$

and the dynamic conditions

$$(\sigma''_{ij})_\tau = (\sigma'_{ij})_\tau + \nabla\gamma(T)|_S,$$
$$(\sigma''_{ij})_n - (\sigma'_{ij})_n = -\gamma(T)\left(\frac{1}{R_1} + \frac{1}{R_2}\right)$$

have to be satisfied. Here, $(\sigma_{ij})_n$ and $(\sigma_{ij})_\tau$ are the normal and tangential components of the stress tensor at the interface, $\gamma(T)$ is the surface tension, which depends on the temperature, R_1 and R_2 are the radii of curvature of the element S of the interface. Eqs. (1) and (2) were solved using the LBE method with phase transitions (see Section 3).

The calculations of electric field were carried out taking into account the change of the permittivity of the binary mixture in time and space. Hence, we solved the following equation for the potential of the electric field φ

$$\mathrm{div}(\varepsilon \mathrm{grad}\,\varphi) = 0. \tag{3}$$

The electric field is equal to $\mathbf{E} = -\nabla\varphi$. The nonlinear dependence of the permittivity ε on the density ρ for nonpolar dielectric liquids was used in simulations:

$$\varepsilon(\rho) = 1 + \frac{3\alpha\rho}{1 - \alpha\rho}. \tag{4}$$

Eq. (3) was solved at each time step by the well-known method of simple iterations Eq. (19) that can be derived from the three-dimensional central finite difference approximation of Eq. (3) (see Section 6).

3. Lattice Boltzmann equation method

The LBE method is successfully applicable for computer simulations of systems with interfaces between vapor and liquid phases. Now the LBE method is widely exploited in simulations of complex fluid flows, including multiphase and multicomponent ones. The advantages of the LBE method are the simplicity of the algorithm, the possibility of parallel computations and an easy implementation of boundary conditions.

In the LBE method, single particle distribution functions N_k are used as variables. The standard evolution equation has the form

$$N_k(\mathbf{x} + \mathbf{c}_k\Delta t, t + \Delta t) = N_k(\mathbf{x}, t) + \Omega_k(N(\mathbf{x}, t)) + \Delta N_k. \tag{5}$$

Here Ω_k is the collision operator, $\mathbf{c}_k$ are the pseudo-particle velocities, and Δt is the time step. The fluid density and the velocity at a node can be calculated as $\rho = \sum_{k=0}^{b} N_k$ and $\rho\mathbf{u} = \sum_{k=1}^{b} \mathbf{c}_k N_k$. The three-dimensional variant of the LBE method D3Q19 [23] with nineteen velocity vectors ($|\mathbf{c}_k| = 0$, 1 or $\sqrt{2}$) on a cubic lattice was realized.

In LBE methods, different phases of a substance are usually simulated as one fluid. In this case, there is no need to track the interfaces between the vapor and liquid phases. These interfaces are represented as thin transition layers of finite width (several lattice nodes) in which the density changes smoothly from one bulk value to another. For the purpose of simulating the transition between phases, the special forces acting on a node were included into the LBE algorithm. These forces implicitly simulated the vapor–liquid coexistence curve and also the surface tension at the interface.

Each time step of the one-component LBE method with phase transitions consists of several substeps implemented sequentially [24,25]:

1. In-place propagation step [19,24] along the characteristics. The propagation performed at the reading of memory was less expensive than at the writing. This type of propagation step has the form

$$\hat{N}_k(\mathbf{x}, t) = N_k(\mathbf{x} - \mathbf{c}_k\Delta t, t - \Delta t). \tag{6}$$

2. Calculation of new values of the density ρ and of the function $\Phi(\rho, T)$ at every node using the specific EOS. In works [11–13], the function $\Phi = \sqrt{-U}$ was introduced, where $U = P(\rho, T) - \rho\theta$ is the pseudopotential. Note that the values under the square root are positive, because the value of U is negative in the basic region of the parameters [24]. Hence we have

$$\rho = \sum_{k=0}^{b} \hat{N}_k \tag{7}$$

$$\Phi = \sqrt{\rho\theta - P(\rho, T)}. \tag{8}$$

3. Calculation of the total force, acting on a node. According to the idea of the pseudopotential proposed in [10], the total force is $\mathbf{F} = -\nabla U$ or in the equivalent form $\mathbf{F} = 2\Phi\nabla\Phi$. Hence, we can write the expression for the force in the new equivalent form

$$\mathbf{F} = (1-2A)2\Phi\nabla\Phi + 2A\nabla(\Phi^2),$$

where A is a free parameter. The appropriate isotropic finite difference approximation of this equation was proposed in [11–13] :

$$\mathbf{F}(\mathbf{x}) = \frac{1}{\alpha h}\left[(1-2A)\Phi(\mathbf{x})\sum_k \frac{G_k}{G_0}\Phi(\mathbf{x}+\mathbf{e}_k)\,\mathbf{e}_k + A\sum_k \frac{G_k}{G_0}\Phi^2(\mathbf{x}+\mathbf{e}_k)\,\mathbf{e}_k\right] \tag{9}$$

To ensure the isotropy of this equation in space, the coefficients G_k should be different for basic and diagonal directions of the lattice. Hence, the coefficients G_k for diagonal directions are equal to $G_0/4$ and $G_0/2$ for the two-dimensional model D2Q9 and the three-dimensional model D3Q19, respectively [26]. For the particular value $A = -0.152$, the coexistence curve (binodal) for the van der Waals equation of state is reproduced in the LBE simulations very accurately in the range from the critical temperature $T_{\rm cr}$ down to the temperature $T = 0.4T_{\rm cr}$ (the deviations from the theoretical values are lower than 0.4% [11–13]).

4a. Calculation of velocities before and after the action of force on a node

$$\rho\mathbf{u} = \sum_{k=1}^{b}\mathbf{c}_k\hat{N}_k, \tag{10}$$

$$\mathbf{u} + \Delta\mathbf{u} = \mathbf{u} + \mathbf{F}\Delta t/\rho. \tag{11}$$

4b. Calculation of the corresponding equilibrium distribution functions [27] that have the form

$$N_k^{\rm eq}(\rho,\mathbf{u}) = \rho w_k\left(1 + \frac{\mathbf{c}_k\mathbf{u}}{\theta} + \frac{(\mathbf{c}_k\mathbf{u})^2}{2\theta^2} - \frac{\mathbf{u}^2}{2\theta}\right). \tag{12}$$

4c. The change of the distribution functions in nodes due to the collision operator (BGK or MRT) Ω_k and $\Delta\hat{N}_k$ is the change due to the total force that includes the external forces

$$N_k(\mathbf{x},t) = \hat{N}_k(\mathbf{x},t) + \Omega_k(\hat{N}(\mathbf{x},t)) + \Delta\hat{N}_k. \tag{13}$$

The collision operator in the BGK approximation has the form

$$\Omega_k = (N_k^{\rm eq}(\rho,\mathbf{u}) - \hat{N}_k(\mathbf{x},t))/\tau. \tag{14}$$

The exact difference method (A.L. Kupershtokh, 2004) [24,28,29] was used for the implementation of the total body force

$$\Delta\hat{N}_k(\mathbf{x},t) = N_k^{\rm eq}(\rho,\mathbf{u}+\Delta\mathbf{u}) - N_k^{\rm eq}(\rho,\mathbf{u}). \tag{15}$$

In present simulations, the van der Waals equation of state is used, which can be written in reduced variables ($\tilde{P} = P/P_{\rm cr}$, $\tilde{\rho} = \rho/\rho_{\rm cr}$ and $\tilde{T} = T/T_{\rm cr}$) as

$$\tilde{P} = \frac{8\tilde{\rho}\tilde{T}}{3-\tilde{\rho}} - 3\tilde{\rho}^2. \tag{16}$$

Here and below, we will use the sign "$\sim$" for all reduced variables.

4. Parallel computations on graphics processing units

To simulate the three-dimensional problems we used modern Graphics Processing Units with NVIDIA "Fermi" architecture. We used several GTX-580 GPUs on a desktop computer, as well as several Tesla M2090 cards on the GPU cluster at the Novosibirsk State University. Each of these GPUs contains 512 processors (cores). All cores of one GPU have a direct access to the fast global device memory (3 GB for GTX-580 and 6 GB for Tesla M2090). The LBE method employs calculations mostly at one single lattice node except for the computations in the propagation step and the computations of the gradient of the pseudopotential. Hence, the parallel implementation of the LBE algorithm can be realized on a large number of cores in a GPU. For the GPU programming we used the CUDA (Compute Unified Device Architecture) technology.

Four kernels corresponding to four main substeps were named *MOVE_f*, *DENSITY*, *FORCE* and *COLLIS*. The relative time of execution of kernels during one time step for the three-dimensional one-component two-phase LBE model D3Q19 is shown on the histogram (Fig. 1), obtained by the standard profiler of CUDA 4.0 [30]. The most time-consuming substeps are the calculations of the four main kernels and the application of boundary conditions along the x coordinate. Other calculations concerning the boundary conditions took less than 1% of the total computational time. The throughput of one GPU GTX-580 for the one-component two-phase LBE model is approximately 80–90 Million Node Updates Per Second (MNUPS).

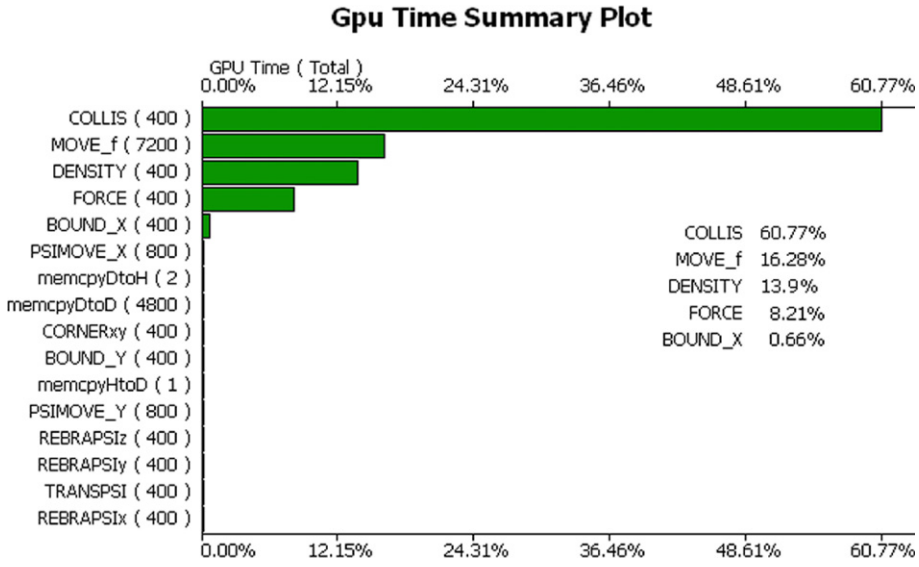

Fig. 1. The relative time of execution of kernels averaged over 400 time steps. Computations using the GTX-580 card on the lattice of 256 × 256 × 192 nodes. The total number of lattice nodes is 12.6 million.

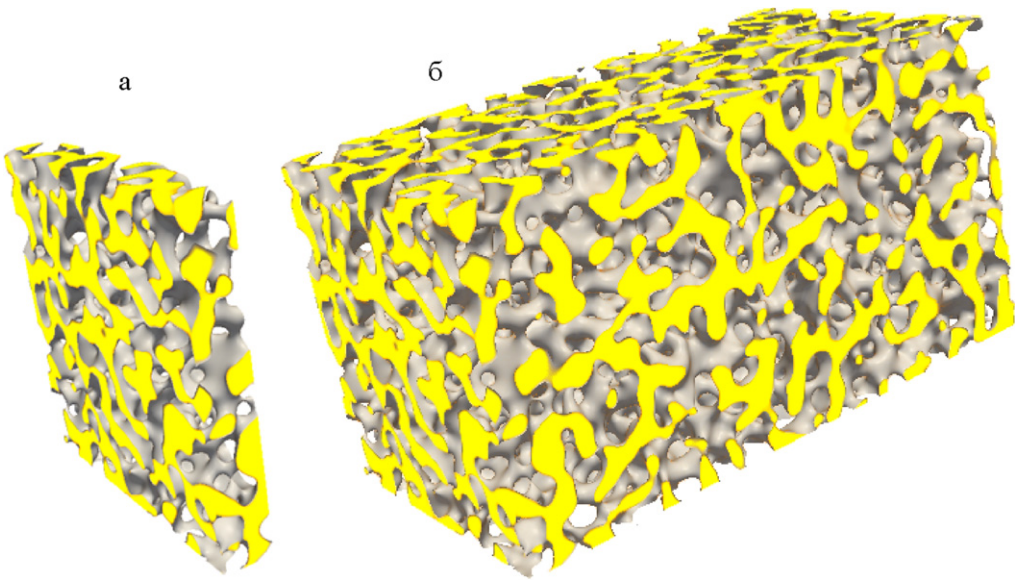

Fig. 2. Simulation of the spinodal decomposition using 12 GPUs. The vapor phase is shown as transparent. $\tilde{T} = 0.7$, $\tilde{\rho}_0 = 1.0$, $\tau = 1$, $t = 2000$. Lattice is 512 × 512 × 960 lattice nodes (more than 250 million). The total throughput is 250 MNUPS. Execution time ≈30 min.

5. Simulations of spinodal decomposition using the lattice Boltzmann equation method

The problem of a spinodal decomposition (decay of uniform fluid with the initial state being under the spinodal curve into the two-phase system vapor–liquid) was used as a three-dimensional test. The example of the three-dimensional simulation of spinodal decomposition is shown in Fig. 2(b). The total computational domain was 512 × 512 × 960 lattice nodes. The periodic boundary conditions were used along all three coordinates x, y and z. In the certain range of an initial density of the fluid, the separation of vapor and liquid phases occurred after some period of time. The liquid phase looks like the "penetrable" porous medium. The small-scale structures were generated at the beginning, but they grew in size as the simulation progressed.

The simulations were carried out on 12 GPUs (Tesla-M2090, each GPU allows one to use up to 5.3 Gb of fast global device memory with ECC) on the hybrid GPU cluster at Novosibirsk State University. The total number of cores was more than 6000. On every GPU the computational volume was 512 × 512 × 80 lattice nodes. The part of the simulation results from the first

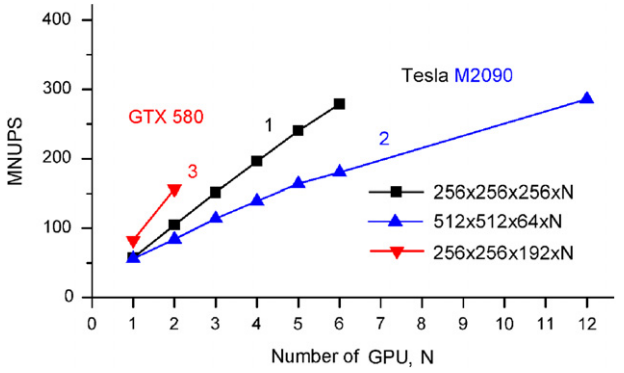

Fig. 3. The throughput of the computations for the three-dimensional one-component variant of the LBE method D3Q19 with phase transitions.

GPU is shown in Fig. 2(a). The boundary conditions along the z coordinate, corresponding to the sides (512×512 nodes), were exchanged between 12 nodes of the cluster using the MPI (Message Passing Interface).

Fig. 3 shows the throughput of computations in Million Node Updates Per Second (MNUPS) for the three-dimensional one-component variant of the LBE method with phase transitions. The results shown by curves 1 and 2 were obtained on the GPU cluster of Novosibirsk State University using the MPI protocol. In these computations, one of the three Tesla M2090 modules was used on each computing node of the cluster. Curve 3 represents the results obtained on a desktop workstation with two GTX 580 devices (each has 3 GB fast global device memory). Throughput of the GTX 580 GPU for the three-dimensional LBE simulations is considerably higher than of the Tesla M2090 GPU.

The computation time of a single LBE step (one-component two-phase model) normalized by the number of grid nodes allocated in one GPU is shown in Fig. 4. It includes the time for data transfer at boundaries between cluster nodes using the MPI protocol. We used only one GPU at every node of the cluster. In the case of the simulations on a single node of the cluster, the boundary conditions along the z coordinate were transferred using the CUDA function "cudaMemcpyPeer()" without using the MPI. If the amount of transferred information using the MPI protocol between two neighbor nodes of the cluster increases fourfold (256×256 for curve 1 and 512×512 for curve 2), the transfer time also approximately quadruples with the same amount of computations at the nodes ($256 \times 256 \times 256 = 512 \times 512 \times 64$). This means that the communication between nodes of the cluster was not realized in parallel. This disadvantage can be overcome. The very simple procedures to transfer the necessary arrays between nodes of the cluster: "MPI_Sendrecv" and "MPI_Barrier" were used here without communication hiding. One can achieve strong scaling with communication hiding.

6. The simulations of a decay of binary mixtures in strong electric fields using the lattice Boltzmann method

In a general case, the body force acting on a dielectric liquid in an electric field in the absence of free charges is given by the Helmholtz formula [31]

$$\mathbf{F} = -\frac{E^2}{8\pi}\nabla\varepsilon + \frac{1}{8\pi}\nabla\left[E^2\rho\left(\frac{\partial\varepsilon}{\partial\rho}\right)_T\right]. \tag{17}$$

The first and the second terms represent the action of an electric field on polarization charges in a nonuniform dielectric and the electrostriction forces.

Earlier in our works [3,4], the new physical effect of anisotropic instability of a pure dielectric liquid in a strong electric field was predicted theoretically and was investigated in two-dimensional computer simulations. Hence, the anisotropic separation of the initially homogeneous fluid into the liquid and vapor phases is possible in strong electric fields for a fluid that is initially in a stable state. It is important that the new regions of low-density phase appear as thin quasi-cylindrical channels oriented along the electric field. This effect can occur for dielectric liquids with a nonlinear density dependence of permittivity $\varepsilon(\rho)$ in an initially uniform electric field $E_z = E_0$ because of the electrostrictive forces

$$F_x = \frac{E_0^2\rho}{8\pi}\left(\frac{\partial^2\varepsilon}{\partial\rho^2}\right)_T\frac{\partial\rho}{\partial x}, \qquad F_y = \frac{E_0^2\rho}{8\pi}\left(\frac{\partial^2\varepsilon}{\partial\rho^2}\right)_T\frac{\partial\rho}{\partial y}, \tag{18}$$

that are perpendicular to the electric field and are directed towards the regions of higher density.

In the present investigation, the three-dimensional simulations of this phenomenon were carried out. For this purpose, we realized the three-dimensional variant of the LBE method for a multicomponent fluid, which is placed in the electric field, with the possibility of vapor–liquid phase transitions. This method also takes into account the pressure dependence of the mutual solubility of components.

The calculations of electric field are carried out taking into account the change of the permittivity of the binary mixture in time and space. Hence, we solved Eq. (3) for the potential of the electric field at each time step. The periodic boundary

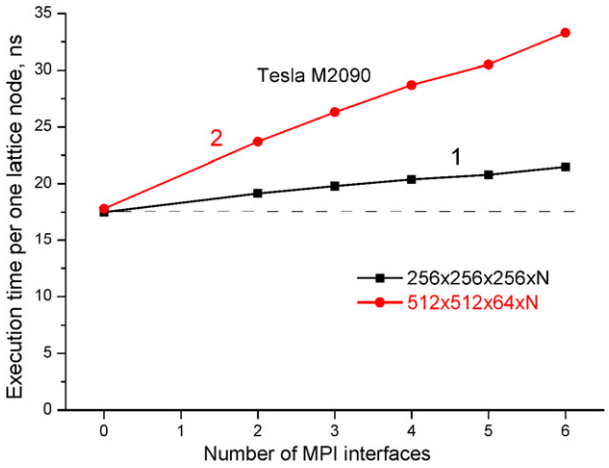

Fig. 4. The computation time of one LBE step normalized per number of grid nodes allocated in a single GPU. For a single node of the cluster, the number of MPI interfaces is equal to zero. For n nodes, the number of MPI interfaces between nodes is equal to n.

conditions are used along the x and y coordinates: $\varphi(0, y, z) = \varphi(L_x, y, z)$ and $\varphi(x, 0, z) = \varphi(x, L_y, z)$ for the calculation domain in the form of a rectangular parallelepiped of dimensions L_x, L_y, L_z. The values of the potential at the two other sides of the calculation domain were given in the form $\varphi(x, y, 0) = V$ and $\varphi(x, y, L_z) = 0$. Hence, the initial electric field was assumed to be uniform $E_z = E_0 = V/L_z$.

From the three-dimensional central finite difference approximation of Eq. (3), one can derive the method of simple iterations that can be written in the form

$$\varphi^{n+1}(\mathbf{x}) = \frac{\sum_{k=1}^{6} (\varepsilon(\mathbf{x}, t) + \varepsilon(\mathbf{x} + \mathbf{c}_k \Delta t, t)) \varphi^n(\mathbf{x} + \mathbf{c}_k \Delta t)}{\sum_{k=1}^{6} (\varepsilon(\mathbf{x}, t) + \varepsilon(\mathbf{x} + \mathbf{c}_k \Delta t, t))}. \tag{19}$$

The values of permittivity ε and the initial values of the potential were taken from the previous time step $\varphi^0(\mathbf{x}) = \varphi(\mathbf{x}, t)$. This approach was a very good initial approximation for iterations because of the density ρ and, consequently, ε does not change noticeably during one time step.

To simulate the binary mixture, two sets of the LBE distribution functions N_k^s and N_k^σ were used. The evolution equations for distribution functions of each component s and σ have the form

$$N_k^{s,\sigma}(\mathbf{x} + \mathbf{c}_k \Delta t, t + \Delta t) = N_k^{s,\sigma}(\mathbf{x}, t) + \Omega_k^{s,\sigma} + \Delta N_k^{s,\sigma}, \tag{20}$$

where $\Omega_k^{s,\sigma} = (N_k^{\mathrm{eq}}(\rho^{s,\sigma}, \mathbf{u}^{s,\sigma}) - N_k^{s,\sigma}(\mathbf{x}, t))/\tau$ is the collision operator in the BGK form (relaxation to the equilibrium state), and

$$\Delta N_k^{s,\sigma} = N_k^{\mathrm{eq}}(\rho^{s,\sigma}, u^{s,\sigma} + \Delta \mathbf{u}^{s,\sigma}) - N_k^{\mathrm{eq}}(\rho^{s,\sigma}, \mathbf{u}^{s,\sigma}) \tag{21}$$

is the change of the distribution functions due to the action of body forces including the forces that ensure the phase transitions [11,13,24,25].

Here $\rho^s = \sum_k N_k^s$ and $\rho^\sigma = \sum_k N_k^\sigma$ are the densities of the components of the mixture, $\mathbf{u}^s = \sum_k N_k^s \mathbf{c}_k/\rho^s$ and $\mathbf{u}^\sigma = \sum_k N_k^\sigma \mathbf{c}_k/\rho^\sigma$ are the velocities of the components at a given node.

The limited solubility of a gas in a liquid was simulated by adding the repulsive forces acting in node i on the substance of each component from the substance of the other component that is present in neighbor nodes k. The total forces acting on the substance of components at a node due to these repulsion forces have the form

$$\mathbf{F}^s(\mathbf{x}) = \psi[\rho^s(\mathbf{x})] \sum_k B_k \psi[\rho^\sigma(\mathbf{x} + \mathbf{e}_k)]\, \mathbf{e}_k,$$

$$\mathbf{F}^\sigma(\mathbf{x}) = \psi[\rho^\sigma(\mathbf{x})] \sum_k B_k \psi[\rho^s(\mathbf{x} + \mathbf{e}_k)]\, \mathbf{e}_k.$$

All coefficients B_k are expressed with one parameter of interaction of components $B < 0$, which specifies the degree of mutual solubility of the components. Here, $\psi(\rho)$ is the increasing function that depends on the density of the corresponding component and determines the dependence of the solubility of components on pressure.

The van der Waals equation of state (16) was used for the dielectric liquid. The usual equation of state of an ideal gas $\tilde{P} = \tilde{\rho}\tilde{T}$ was used for the solute gas.

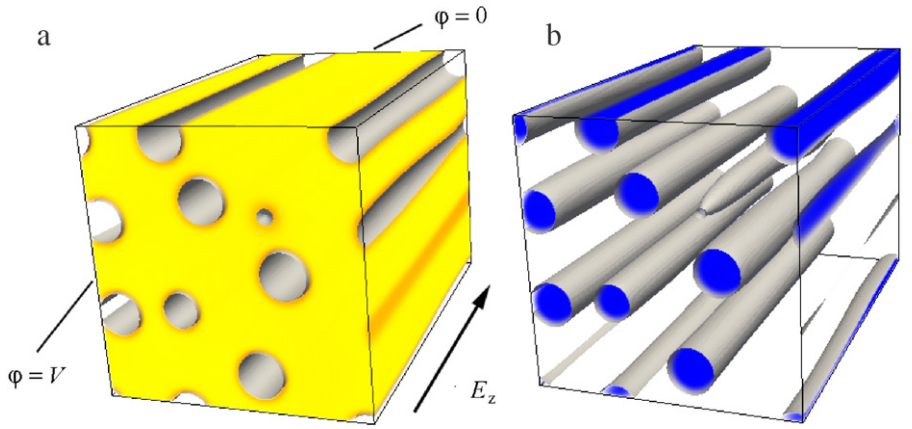

Fig. 5. The decay of a binary mixture in the three-dimensional electric field. (a) Dielectric liquid, (b) gas–vapor channels. $\tilde{T} = 0.9$, $\tilde{\rho}_0 = 1.66$, $\tilde{A} = 30$, $B = -0.02$, $q = 0.02$, $\tau = 1$, $t = 6000$. Lattice $160 \times 160 \times 256$.

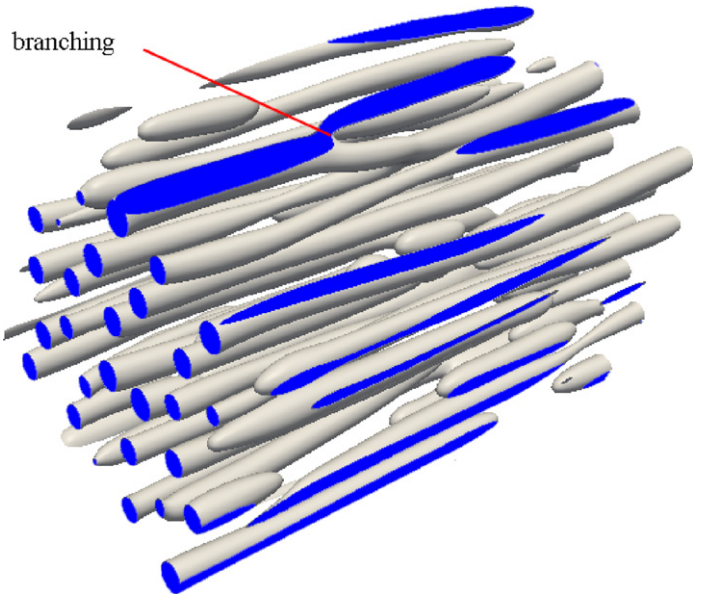

Fig. 6. The decay of a binary mixture in the three-dimensional strong electric field. Only the gas–vapor channels are shown. $\tilde{T} = 0.9$, $\tilde{\rho}_0 = 1.66$, $\tilde{A} = 60$, $B = -0.02$, $q = 0.02$, $\tau = 1$, $t = 1800$. The lattice is $192 \times 192 \times 352$.

For three-dimensional simulations of the full problem (a binary mixture with possible phase transitions and the electric field potential), the lattices up to $160 \times 160 \times 256$ nodes can be allocated on one GTX-580 GPU (3 GB device memory). The computations of the potential of the electric field in accordance with Eq. (3) using the simple iteration method can be easily implemented as a parallel algorithm on the GPU.

The results of three-dimensional simulations of the decay of an initially uniform binary mixture of a dielectric liquid and solute gas into separate components under the action of high electric field are shown in Fig. 5. This simulation was carried out on one GPU (GTX-580). The initial state of the fluid corresponds to the liquid state on the saturation curve at a given temperature. At any local small decrease of density due to stochastic perturbations, the pressure in this local volume decreases due to the electrostrictive forces even more. Hence, the solubility of gas in the liquid in this local region also decreases. The process of gas liberation leads to a further increase of the density gradient. Thus, the process of the gas liberation in the form of gas–vapor channels oriented on the average along the electric field has a bursting character. The process of decay is determined by the dimensionless magnitude of the electric field squared $\tilde{A} = E_0^2/(8\pi P_{cr})$ [3] and by the reduced temperature $\tilde{T}$. The initial states of the binary mixture at every temperature usually correspond to the liquid states on the saturation curve.

The gas–vapor channels expand because of the diffusion of the solute gas from the mixture, the evaporation of liquid into the channels and also due to the coalescence of the channels with each other. It is well known from experimental investigations devoted to the breakdown of dielectric liquids that the stronger the electric field, the larger the number of

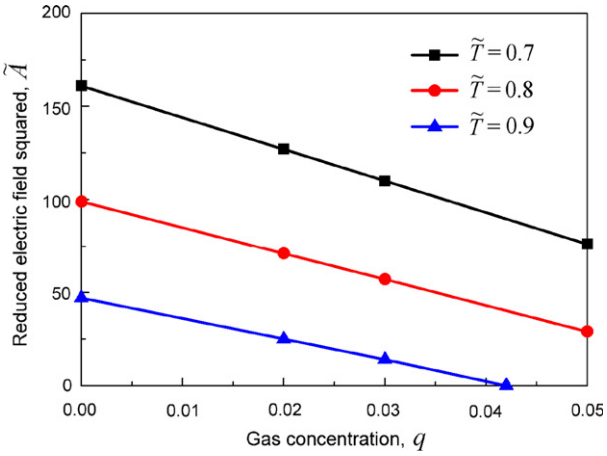

Fig. 7. The dependences of the critical values of a reduced electric field squared on initial concentration of solute gas q. The initial states of the binary mixture at every temperature correspond to the liquid states on the saturation curve. $B = -0.02$, $\tau = 1$.

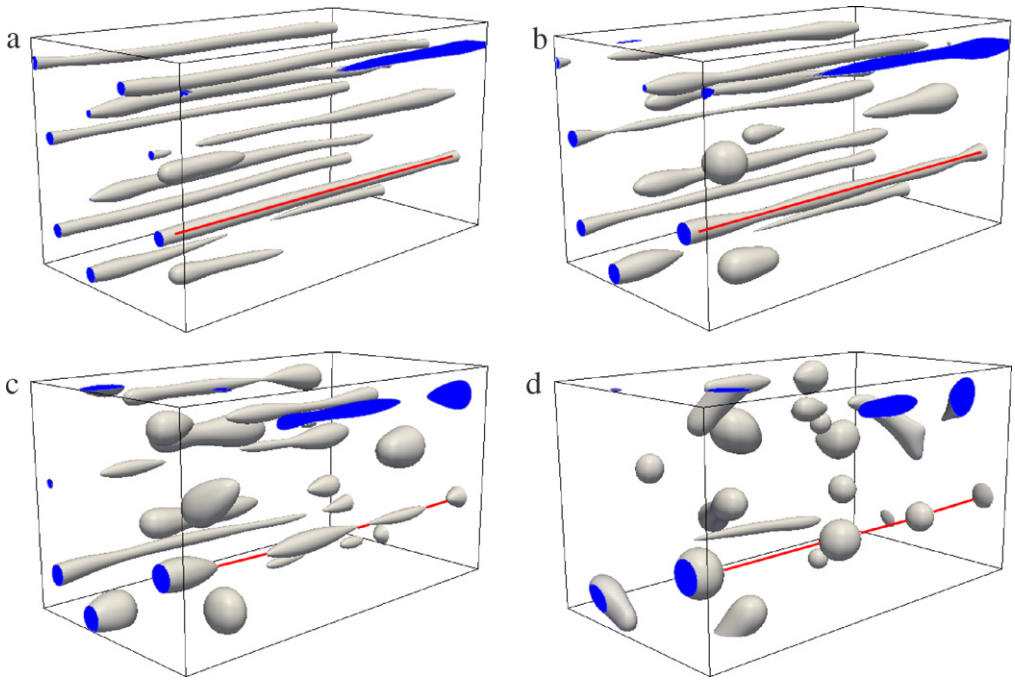

Fig. 8. The decay of the gas–vapor channels after turning off the electric field. Only the gas–vapor channels are shown. $\tilde{T} = 0.9$, $\tilde{\rho}_0 = 1.66$, $\tilde{A} = 30$, $B = -0.02$, $q = 0.02$, $\tau = 1$. The lattice is $192 \times 192 \times 352$. $t = 5600$ (a); 6600 (b); 7600 (c); 9000 (d).

streamer channels generated in the same volume of liquid. This effect was reproduced particularly well in our simulations (Fig. 6). At the first stage, the gas–vapor channels have a form close to cylindrical. In some places, the branching of channels can be observed (Fig. 6). This simulation was carried out on two GPUs (GTX-580) on the desktop computer.

Fig. 7 shows the dependences of the critical values of the reduced electric field that are necessary for anisotropic decay of binary mixtures of the dielectric liquid and solute gas into components on the initial concentration of solute gas q at different temperatures. The initial states of the binary mixture at every temperature correspond to the liquid states on the saturation curve: $\tilde{\rho}_0 = 2.14$ at $\tilde{T} = 0.7$, $\tilde{\rho}_0 = 1.93$ at $\tilde{T} = 0.8$, and $\tilde{\rho}_0 = 1.66$ at $\tilde{T} = 0.9$. The increase in the initial concentration of the solute gas considerably decreases the critical values of the uniform electric field at which the anisotropic mechanism of generation and growth of streamer channels operates. Moreover, the closer the state of the mixture is to a critical point; the weaker the critical electric field required to separate the binary mixture into components.

Thus, the critical values of the electric field necessary for such a decay of a binary mixture are considerably less than for the pure dielectric liquids. Hence, if we take into account a solute gas, the electric fields for which the anisotropic mechanism of streamer channels generation and growth is operated become considerably weaker.

These channels are unstable. Hence, after turning off the electric field, every channel decays into the linear chain of small bubbles (Fig. 8). The time of a channel decay into the chain of bubbles due to the constriction instability depends on the channel radius and the surface tension. This simulation was carried out on two GPUs (GTX-580) on the desktop computer.

7. Conclusions

The three-dimensional simulations of anisotropic decay of binary mixtures of a dielectric liquid with solute gas in a strong electric field were carried out. The Lattice Boltzmann Equation method was exploited for computer simulations of the evolution of such systems with the newly arising interfaces between vapor and liquid phases. The parallel implementation of the LBE algorithm was realized on a large number of cores in the GPU. For the GPU programming, the CUDA technology was used.

It is important that new regions of low-density phase appear as thin quasi-cylindrical gas–vapor channels oriented along the electric field. The gas–vapor channels expand because of the diffusion of the solute gas from the mixture, evaporation of liquid into the channels and also due to the coalescence of channels with each other. The critical values of electric field necessary for such decay of a binary mixture are considerably lower than for pure dielectric liquids. Hence, if we take into account a solute gas, the electric fields for which the anisotropic mechanism of streamer channels generation and growth is operated become considerably lower.

Thus, at a breakdown of dielectric liquids in a strong electric field, the anisotropic instability is possibly the key mechanism of the generation of a gas phase, inception of conducting streamer structures, their fast growth in the form of thin filamentary channels, as well as branching of streamer structures during propagation.

References

[1] E.V. Yanshin, I.T. Ovchinnikov, Yu.N. Vershinin, Mechanism of the pulsed electrical breakdown of water, Sov. Phys. Dokl. 19 (2) (1974) 95–96.
[2] O. Lesaint, G. Massala, Positive streamer propagation in large oil gaps. Experimental characterization of propagation modes, IEEE Trans. Dielectr. Electr. Insul. 5 (2) (1998) 360–370.
[3] A.L. Kupershtokh, D.A. Medvedev, Anisotropic instability of a dielectric liquid in a strong uniform electric field: decay into a two-phase system of vapor filaments in a liquid, Phys. Rev. E 74 (2) (2006) 021505.
[4] D.I. Karpov, A.L. Kupershtokh, Anisotropic spinodal decomposition of a polar dielectric in a strong electric field: molecular dynamics simulations, Tech. Phys. Lett. 35 (5) (2009) 479–482.
[5] W. An, K. Baumung, H. Bluhm, Underwater streamer propagation analyzed from detailed measurements of pressure release, J. Appl. Phys. 101 (5) (2007) 053302.
[6] A.L. Kupershtokh, D.I. Karpov, Simulation of ultra-fast streamer growth governed by the mechanism of anisotropic decay of a dielectric liquid into a liquid–vapor system in high electric fields, in: Proc. 5th Conf. SFE, Grenoble, France, 2006, pp. 179–184.
[7] A.K. Gunstensen, D.H. Rothman, S. Zaleski, G. Zanetti, Lattice Boltzmann model of immiscible fluids, Phys. Rev. A 43 (1991) 4320–4327.
[8] M.R. Swift, W.R. Osborn, J.M. Yeomans, Lattice Boltzmann simulations of nonideal fluids, Phys. Rev. Lett. 75 (5) (1995) 830–833.
[9] X. Shan, H. Chen, Lattice Boltzmann model for simulating flows with multiple phases and components, Phys. Rev. E 47 (3) (1993) 1815–1819.
[10] Y.H. Qian, S. Chen, Finite size effect in lattice-BGK models, Internat. J. Modern Phys. C 8 (4) (1997) 763–771.
[11] A.L. Kupershtokh, Simulation of flows with liquid–vapor interfaces by the lattice Boltzmann method, Vestnik NGU (Quarterly Journal of Novosibirsk State Univ.), Series: Math., Mech. and Informatics 5 (3) (2005) 29–42 (in Russian).
[12] A.L. Kupershtokh, D.I. Karpov, D.A. Medvedev, C. Stamatelatos, V.P. Charalambakos, E.C. Pyrgioti, D.P. Agoris, Stochastic models of partial discharge activity in solid and liquid dielectrics, IET Sci. Meas. Technol. 1 (6) (2007) 303–311.
[13] A.L. Kupershtokh, D.A. Medvedev, D.I. Karpov, On equations of state in a lattice Boltzmann method, Comput. Math. Appl. 58 (5) (2009) 965–974.
[14] R. Zhang, H. Chen, Lattice Boltzmann method for simulations of liquid–vapor thermal flows, Phys. Rev. E 67 (6) (2003) 066711.
[15] S. Gong, P. Cheng, Numerical investigation of droplet motion and coalescence by an improved lattice Boltzmann model for phase transitions and multiphase flows, Comput. Fluids 53 (2011) 93–104.
[16] W. Li, X. Wei, A. Kaufman, Implementing lattice Boltzmann computation on graphics hardware, Vis. Comput. 19 (2003) 444–456.
[17] J. Tölke, M. Krafczyk, TeraFLOP computing on a desktop PC with GPU for 3D CFD, Int. J. Comput. Fluid Dyn. 22 (7) (2008) 443–456.
[18] C. Janßen, M. Krafczyk, Free surface flow simulations on GPGPU using the LBM, Comput. Math. Appl. 61 (12) (2011) 3549–3563.
[19] C. Obrecht, F. Kuznik, B. Tourancheau, J.-J. Roux, A new approach to the lattice Boltzmann method for graphics processing units, Comput. Math. Appl. 61 (12) (2011) 3628–3638.
[20] C. Obrecht, F. Kuznik, B. Tourancheau, J.-J. Roux, Multi-GPU implementation of the lattice Boltzmann method, Comput. Math. Appl. 65 (2) (2013) 252–261.
[21] S.D.C. Walsh, J. Myre, M.O. Saar, D.J. Lilja, Multi-GPU, multi-core, multi-phase lattice-Boltzmann simulations of fluid flow for the geosciences, in: Eos Trans. American Geophysical Union, Fall Meeting Supplement, 2009. Abstract #H23D-0983.
[22] S.D.C. Walsh, M.O. Saar, Developing extensible lattice-Boltzmann simulators for general-purpose graphics-processing units, Commun. Comput. Phys. 13 (3) (2013) 867–879.
[23] Y.H. Qian, S.A. Orzag, Lattice BGK models for the Navier–Stokes equation: nonlinear deviation in compressible regimes, Europhys. Lett. 21 (1993) 255–259.
[24] A.L. Kupershtokh, Criterion of numerical instability of liquid state in LBE simulations, Comput. Math. Appl. 59 (7) (2010) 2236–2245.
[25] A.L. Kupershtokh, Three-dimensional simulations of two-phase liquid–vapor systems on GPU using the lattice Boltzmann method, in: Numerical Methods and Programming: Section 1, in: Numerical Methods and Applications, vol. 13, 2012, pp. 130–138 (in Russian).
[26] N.S. Martys, H. Chen, Simulation of multicomponent fluids in complex three-dimensional geometries by the lattice Boltzmann method, Phys. Rev. E 53 (1) (1996) 743–750.
[27] J.M.V.A. Koelman, A simple lattice Boltzmann scheme for Navier–Stokes fluid flow, Europhys. Lett. 15 (6) (1991) 603–607.
[28] A.L. Kupershtokh, New method of incorporating a body force term into the lattice Boltzmann equation, in: Proc. of the 5th International EHD Workshop, Poitiers, France, 2004, pp. 241–246.
[29] A.L. Kupershtokh, Incorporating a body force term into the lattice Boltzmann equation, Vestnik NGU (Quarterly Journal of Novosibirsk State Univ.), Series: Math., Mech. and Informatics 4 (2) (2004) 75–96 (in Russian).
[30] NVIDIA CUDA C. Programming guide. Version 4.0. 2011.
[31] L.D. Landau, E.M. Lifshitz, Electrodynamics of Continuous Media, Pergamon Press, Oxford, 1959.